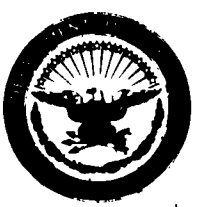

(5) 150 700 64-5

(1)

U. S. Army Ordnance
Ballistics Research Laboratory
Aberdeen Proving Ground, Maryland
Approved Proposal No. 3175
Authorization No. 4086

EXPLOSIVES RESEARCH CENTER

HYPERVELOCITY IMPACT PHENOMENA

Quarterly Report
June 1, 1963 to August 31, 1963

BUREAU OF MINES, PITTSBURGH, PA.

UNITED STATES
DEPARTMENT OF
THE INTERIOR

C 150 700

HYPERVELOCITY IMPACT PHENOMENA

Quarterly Report, 15 June - 31 Aug 63.

June 1, 1963 to August 31, 1963

Prepared for:

U. S. Army Ordnance
Ballistic Research Laboratory
Aberdeen Proving Ground, Maryland
Approved Proposal No. 3175
Authorization No. 4086

by

Richard W. Watson
Karl R. Becker
J. Edmund Hay
Frank C. Gibson,

Approved by:

Robert W. Van Dolah
Research Director
Explosives Research Center

U. S. Department of the Interior
Bureau of Mines
Pittsburgh, Pa.
September 24, 1963

HYPERVELOCITY IMPACT PHENOMENA

Introduction

A considerable amount of information dealing with the penetration of thin metallic targets by high velocity projectiles was accumulated and summarized in a previous report[1/]. Certain concepts, based upon experiments carried out with systems that provided projectile velocities in the range of 2.0 to 5.0 km/sec, were established; however, the applicability of these concepts to higher impact velocities are being determined. Recently, projectile velocities have been extended to about 9.3 km/sec through the use of a projectile produced by a modified shaped charge; the projector system was developed at the Ballistic Research Laboratories, Aberdeen Proving Ground, Maryland.

This report deals with preliminary experiments using projector systems of this type and, where possible, results are compared with those obtained using projectiles in the lower velocity range.

Experimental Procedures and Results

Hypervelocity projectiles, having a velocity of about 9.3 km/sec at impact and a nominal mass of 4 gm, were used in order to determine the spatial distribution of spall numbers and masses as well as the relationship between various parameters and spall particle size. The study consisted of impacts into three different thicknesses of three different target materials. The target thicknesses were 1/8 in, 1/2 in, and 2 in; the target materials

---

1/ Watson, R. W., K. R. Becker, J. E. Hay, and F. C. Gibson, "Hypervelocity Impact Phenomena", Bureau of Mines Quarterly Report, U. S. Army Ordnance, Aberdeen Proving Ground, Md., March 1, 1963 to May 31, 1963.

were 2024-T3 aluminum, AZ31BH-24 magnesium, and 4130 steel. The spall particles were recovered from a target consisting of a stack of 1/2-inch thick fiberboard sheets; the witness target is located ten inches beyond the metal target.

Inhibited Jet Projector

A sketch of the component parts of the Scale I, 9.3 km/sec projector system is shown in figure 1. The projector is of the inhibited jet type and is based on well-known shaped charge principles. Ordinarily, the collapse of the aluminum liner would produce an elongated jet having a peak velocity of about 9.5 km/sec at the front, decreasing to about 2 to 3 km/sec at the rear. However, the collapse process is inhibited by the presence of a Lucite plug inserted into the interior of the cone and only a short portion of the high velocity jet tip is formed for use as a hypervelocity projectile. A hemi-cylindrical diverter charge (Composition B) is affixed to the exterior of the main charge near the base; it is sympathetically initiated and laterally disperses debris that follows the high-speed projectile on its path toward the target. The aluminum cone has a 42° apex angle, 0.120 in-wall thickness, and an interior base diameter of 3.307 inches. A 3.4-inch diameter x 5-1/2-inch long Composition B charge is cast around the cone. A radiograph of the projectile taken 20 inches from the base of the charge is shown in figure 2. At this distance, the projectile velocity, based on nine measurements, is 9.3 km/sec; although the actual distance to the target was 40 inches, the velocity at impact is believed to be little changed. Estimates of the projectile masses were made by measuring the dimensions of the projectile from radiographs and correcting them for magnification (about 11% linear magnification); it was assumed that the projectile was homogeneous material having the density of aluminum. The average mass at the

20-inch distance, based upon six trials, was 3.4 grams. Due to erosion, the masses would be somewhat less at the impact distance of 40 inches. On the basis of one measurement, erosion mounted to roughly 10%; thus, the mass of the projectile at impact is estimated to be about 3.1 grams.

Target Perforation Characteristics

Target perforation diameters and exit spall diameters were measured and the data, supported by one trial for each impact situation, are plotted in figure 3. The independent variable in both plots is target thickness; the dependent variable is entrance or exit diameter in the upper plot and exit spall diameter in the lower plot. The independent parameter is target material (aluminum, magnesium, or steel). The most significant aspect of these data is that the results are qualitatively similar to those obtained from 5.0 km/sec projectiles impacting the same target materials; the 5.0 km/sec data are plotted in figure 4. For both projectile velocities, the spall diameters become increasingly more distinct from the perforation diameters as target thicknesses increase. Furthermore, at given target thickness, both figures show the same correlation between diameter (perforation or spall) and the strength characteristics of the target material; magnesium targets produced the largest diameters and steel targets produced the smallest diameters.

Spatial Distribution of Numbers and Masses of Spall Particles

An attempt was made to recover individual spall particles from the stacks of fiberboard witness sheets; the recovery of individual spall particles, together with their locations in the witness material, provides, in principle, a maximum amount of information from a minimum number of firings. Initially, the paths of the larger

particles were traced through the stack until the particle was located; however, in order to recover relatively small particles, it finally became necessary to pulverize the witness material.

Usable data for the radial distribution of spall numbers and masses were obtained for impacts into 2-inch thick magnesium and aluminum targets. The projectile did not penetrate 2-inch thick steel targets; a spall was produced, however, but the particles were too large and too few in number to be meaningful. Data from impacts into 1/8 in and 1/2 in targets, although useful for other purposes, cannot be normalized by the total number (N) or total mass (M) because of the loss of spall particles from areas of the recovery material at and near the center of impact caused by a rather violent disruption of the witness material.

The data for 2-inch target thicknesses are given in table 1 and plotted in figures 5 and 6. The upper plot shows the normalized distribution of spall numbers while the lower plot shows a similar distribution for spall mass. Both distributions are plotted against solid angle (Ω) - a radially sensitive coordinate. The solid curves in both plots represent previously[2/] published data for 3.2 and 4.0 km/sec projectile impacts into aluminum targets. The available data from 9.3 km/sec impacts appear to be distributed in a manner similar to that observed for lower velocity impacts; maximum density (number or mass) occurs at the center of impact and diminishes radially outward in about the same manner.

Another type of distribution that may be considered is that of spall numbers and spall masses according to depth of penetration into fiberboard witness material. Variation in depth is in terms of one-half inch increments of fiberboard. Analysis was

---

2/ See work cited in footnote 1.

made for impacts into three thicknesses of aluminum target material and into two thicknesses of magnesium target material. The data for aluminum are given in table 2 and plotted in figures 7 and 8. Figure 7 gives the percent of the total number of spall particles as a function of penetration depth into the witness material and figure 8 is a similar representation for the spall mass. Data for magnesium are also given in table 2 and plotted in figures 9 and 10.

Several features that apply to both the aluminum and magnesium data are worthy of consideration: (a) The curves are maximum at the one-half inch penetration level and decrease monotonically with increasing penetration depth into the fiberboard. Only the distribution curve, in figure 8, for spall mass resulting from impacts into 2-in aluminum targets deviates from this form; these data are possibly erratic because of an insufficient sample size. (b) The distribution of numbers and masses of spall particles is found to be a function of target thickness. The percentage of the total spall numbers or mass captured by the first one-half inch thick sheet of recovery material is maximum for impacts into the thinnest metal targets; the percentage decreases with increasing target thickness. For example, the percentages of the total number of aluminum particles captured by the first recovery sheet for impacts into 1/8-in, 1/2-in, and 2-in thick aluminum targets were about 95%, 81%, and 55% respectively. Similar correlations are noted for the aluminum mass data and for all the magnesium data. The correlation must, of course, reverse itself at some greater depth of penetration; the reversal occurs at the second increment of depth in all cases as may be seen by inspecting the plots. (c) One other interesting observation is that spall particle size increases with depth of penetration. This becomes clearly evident when one compares a particular number distribution curve with its

corresponding mass distribution curve. For impacts into 1/8-in aluminum targets, 95% of the total number of particles are represented by only 72% of the total mass at the first penetration level, 4% of the total number contain 21% of the total mass at the second penetration level, and 1% of the total number contain 6% of the total mass at the third penetration level. Similar comparisons are noted for the other impacts. This aspect of the data is more fully discussed in a later section on spall particle size.

Effects of Target Anisotropics on Spall Distribution

Since the target materials used were from rolled stock, certain directional characteristics are incorporated in the target structure which could conceivably influence dispersal of spall products. The orientation of the rolling direction was recorded for all target-recovery sheet setups and the data were examined for possible non-uniformities in the angular dispersal of spall particles. The results of this investigation for impacts into three thicknesses of aluminum targets are presented in figure 11 which is essentially a plot of the percentage of spall particles found in circular sectors having different orientations relative to the rolling direction. A zero slope of the curves would indicate that the particles are evenly distributed around the center of impact; this is apparently not the case because the data point sets for impacts into all three thicknesses of aluminum indicate that there is a tendency for a greater than proportionate share of the total number to be dispersed in the rolling direction. This tendency, although apparently significant, is not particularly marked since sectors adjacent to the rolling direction, which represents one-third of the total area, contain only about 40% rather than 33% of the spall population. It is interesting to note, however, that the distribution of spall particles is influenced by

small differences in the mechanical properties of the material. No significant influence of rolling direction was noted for impacts into magnesium or steel.

Spall Particle Size

Average spall particle size was investigated as a function of target thickness, radial distance from the center of impact, and depth of penetration into the recovery material. The results obtained are as follows:

(1) The effect of target thickness on spall particle size is shown in figure 12; the data are given in table 3. For cases where the center of impact area was severely damaged, analysis was made of undamaged areas of the witness sheets. Curves are shown for aluminum and magnesium targets. The curve for aluminum shows average spall particle size increasing from about 6 mg for 1/8-in thick targets to about 190 mg for 2-in thick targets or by roughly a factor of 30. This observation is qualitatively similar to previous results obtained from impacts into aluminum at 3.2 and 4.0 km/sec[3/]. The figure also includes a curve for magnesium impacts and again it is evident that size increases with target thickness from about 9 mg for 1/8-in thick targets to about 62 mg for 2-in thick targets. The increase in size is not as great as that observed for aluminum and no comparison is available with impacts at lower velocities. Impacts into 2-in thick steel targets are given in table 3 but fall beyond the limits of the plot--the projectile did not penetrate the target; spallation did occur however and produced large particles that averaged about 13 gm. No data are available for lesser thicknesses of steel because many of the spall particles appeared to disintegrate into innumerable particles of extremely small size on im-

3/ Becker, K. R., R. W. Watson, F. C. Gibson, "Hypervelocity Impact Phenomena", Bureau of Mines Quarterly Report, U. S. Army Ordnance, Aberdeen Proving Ground, Md., March 1, 1962 to May 31, 1962.

pacting the witness target.

Summarizing the preceding results, the available data demonstrate the following characteristics: spall particle size increases markedly with increases in target thickness; this is tantamount to stating that size varies inversely with the peak pressure incident on the bottom surface of the target. Also, spall particle size, at given target thickness, varies with target material; average spall particle size was 62 mg, 190 mg, and 13 gm (13,000 mg) for 2-in thick magnesium, aluminum, and steel targets respectively. This effect may, to some extent, be another manifestation of a pressure effect because of differences in peak incident pressure as well as an effect due to the difference in physical properties of the materials. The relative importance of these effects is not yet known.

(2) The relationship between spall particle size and the radial spatial coordinate was investigated for the three aluminum impacts and for two of the magnesium impacts. Although it was not possible to recover all of the spall particles because of damage to the recovery material, those available were used as a basis for size determination. The data are given in table 4 and plotted in figure 13. The figure shows spall particle size normalized by target thickness (so that all available data could be included on one plot) as a function of the radial distance from the center of impact; the dispersion angle is given at the top of the plot. Considering the data as plotted, one cannot justify a monotonic increase or decrease in particle size as the radial coordinate is increased. The data admittedly are somewhat erratic to an extent where it would be difficult to interpret differences by a factor of two. In any event, the changes in particle size incurred by changes in the radial coordinate are small relative to those incurred by changes in target thickness.

(3) Lastly, an attempt was made to investigate the relationship between spall particle size and depth of penetration into fiberboard witness material. The results are shown in figure 14 which gives spall particle size normalized by target thickness as a function of penetration depth for five impact situations involving aluminum and magnesium targets. The data are given in table 5. Despite a few inconsistencies, the data, as a whole, show a tendency for spall particle size to increase progressively with depth of penetration. This does not necessarily imply that the larger particles have higher velocities since the depth of penetration can be expected to be a function of both particle mass and impact velocity[4/].

4/ Whiteford, C. W. and J. M. Regan, "The Determination of the Striking Velocity of Steel Fragments by Their Mass and Penetration into Witness Material", BRL Memorandum Report No. 1333, Aberdeen Proving Ground, Md., April 1961.

TABLE 1. - Data pertaining to the manner in which spall numbers and masses are distributed radially outward.

Ring	Solid Angle (Ω)	$\frac{1}{N}\frac{\Delta N}{\Delta \Omega}$	$\frac{1}{M}\frac{\Delta M}{\Delta \Omega}$
Aluminum Target (2 inches thick)			
1, 2, 3	0.27	1.0	0.88
4	1.14	0.12	0.34
5	1.61	0.04	0.06
6	2.06	0.03	0.05
Magnesium Target (2 inches thick)			
1, 2	0.12	1.8	1.4
3	0.66	0.15	0.20
4	1.14	0.13	0.20
5	1.61	0.03	0.20
6	2.06	0.00	0.00

Notes: (1) Rings are a family of concentric circles whose centers lie at the center of spall impact on the fiberboard recovery sheet (Δ r = 2 in).

(2) $1/N\ \Delta N/\Delta\Omega$ is the population density ($\Delta N/\Delta\Omega$) normalized by the total number (N) of spall particles.

(3) $1/M\ \Delta M/\Delta\Omega$ has a similar interpretation for the spall mass.

(4) The targets were impacted by Scale I, 9.1 km/sec inhibited jet, aluminum, projectiles.

TABLE 2. - Data pertaining to the distribution of spall numbers and masses relative to their depth of penetration into fiberboard recovery sheets.

	Percent of Total Number or Mass Found at Indicated Depth									
	% of Total Number					% of Total Mass				
Depth (in) ⟶	0.5	1.0	1.5	2.0	2.5	0.5	1.0	1.5	2.0	2.5
Target (al.)										
1/8 in.	95%	4%	1%	-	-	72%	21%	6%	-	-
1/2 in.	81	15	3	-	-	59	29	9	2%	1%
2 in.	55	17	15	10%	2%	12	37	20	29	3
Target (mg.)										
1/8 in.	96%	4%	-	-	-	82%	16%	-	-	-
2 in.	44	23	17%	8%	8%	35	30	21%	8%	6%

Notes: (1) The recovery material (witness target) was in the form of a stack of 1/2-inch thick Maftex fiberboard sheets.

(2) A particle found trapped in the first 1/2-inch thick sheet of fiberboard recovery material was considered to have penetrated 1/2 inch of the material etc.

TABLE 3. - Data pertaining to the relationship between spall particle size and target thickness.

Target Material	Average Spall Particle Size (mg)		
	Target thickness (in)		
	(1/8)	(1/2)	(2)
Aluminum (2024-T3	6.0	18.6	189.0
Magnesium (AZ-31B-H24)	12.6	-	62.0
Steel (4130)	-	-	13.0 (gm)

TABLE 4. - Data pertaining to the relationship between spall particle size and the radial spatial coordinate.

Average Spall Particle Size (mg)			
	Aluminum Targets		
Ring	(1/8 in)	(1/2 in)	(2 in)
D.A.	7.0	22.5	145
4	6.4	10.1	507
5	4.4	21.4	285
6	6.6	28.8	316
Others	9.1	43.5	-

	Magnesium Targets	
Ring	(1/8 in)	(2 in)
D.A.	5.1	7.8
4	7.1	10.9
5	6.2	16.7
6	3.1	
Others	12.4	27.6

Notes: (1) D.A. denotes spall particles found in damage area.

(2) Rings are concentric circles about center of impact with $\Delta r = 2$ inches.

(3) Distance between target plate and fiberboard recovery material was 10 inches.

TABLE 5. - Data pertaining to spall particle size relative to penetration into fiberboard recovery sheets.

	Average Spall Particle Size (mg)				
Depth (in) ——→	0.5	1.0	1.5	2.0	2.5
Target (aluminum)					
1/8 in.	4.3	28.8	69.5	-	-
1/2 in.	12.2	31.3	47.1	-	-
2 in.	76.1	766.2	453	1,003	-
Target (magnesium)					
1/8 in.	5.0	28.5		-	-
2 in.	78	128	121	96	

Note: The data listed above were obtained from undamaged areas of the recovery material.

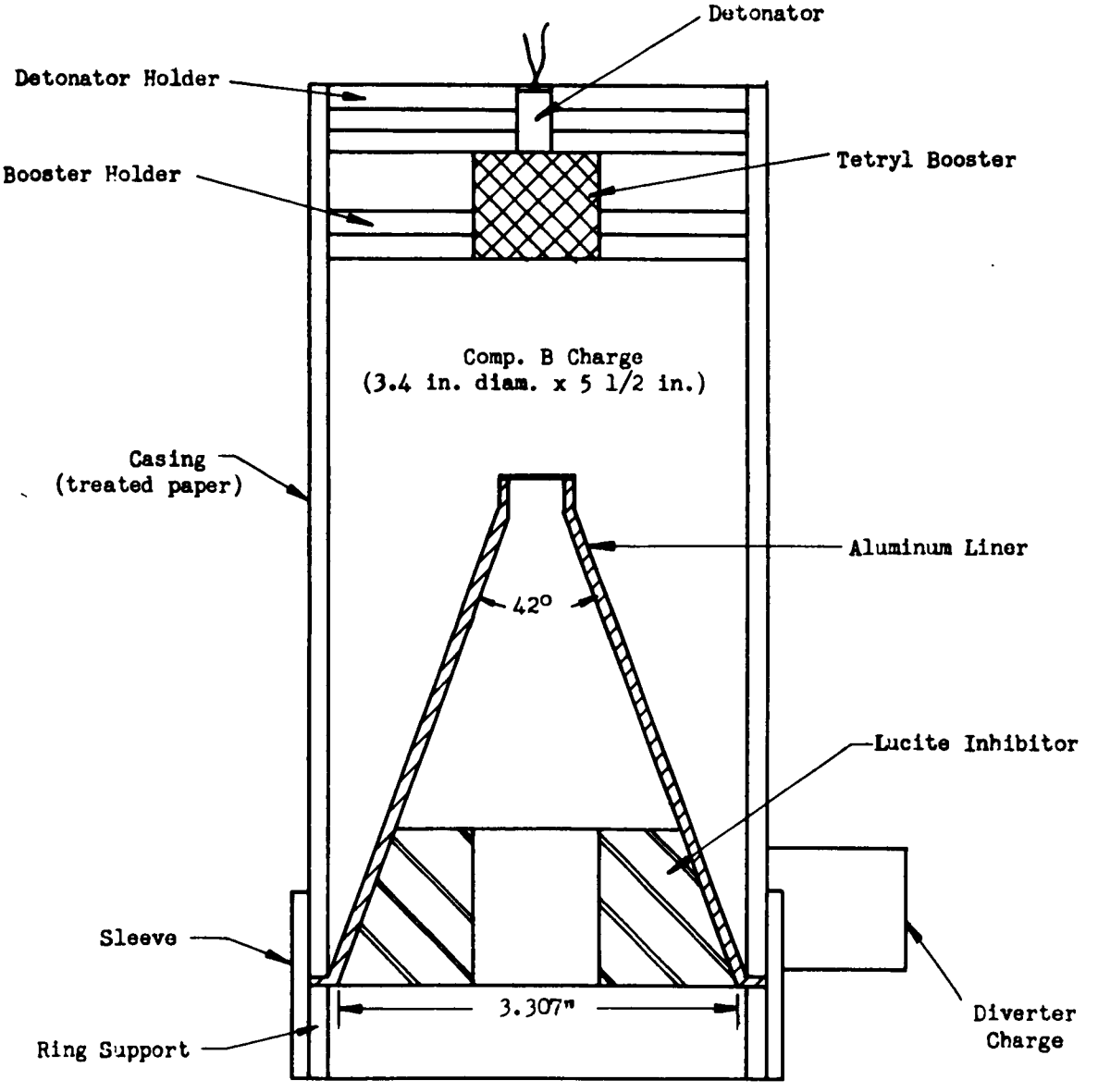

FIGURE 1.- Sketch of Scale I, 9.3 km/sec inhibited jet projector.

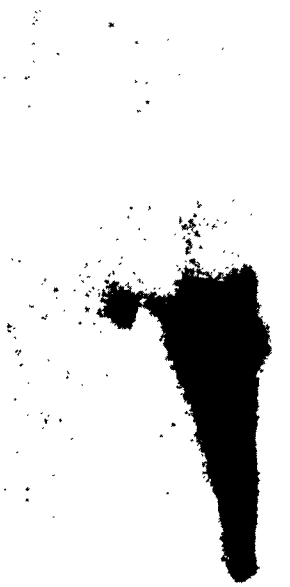

FIGURE 2. - Radiograph of a scale I, 9.3 km/sec inhibited jet projectile.

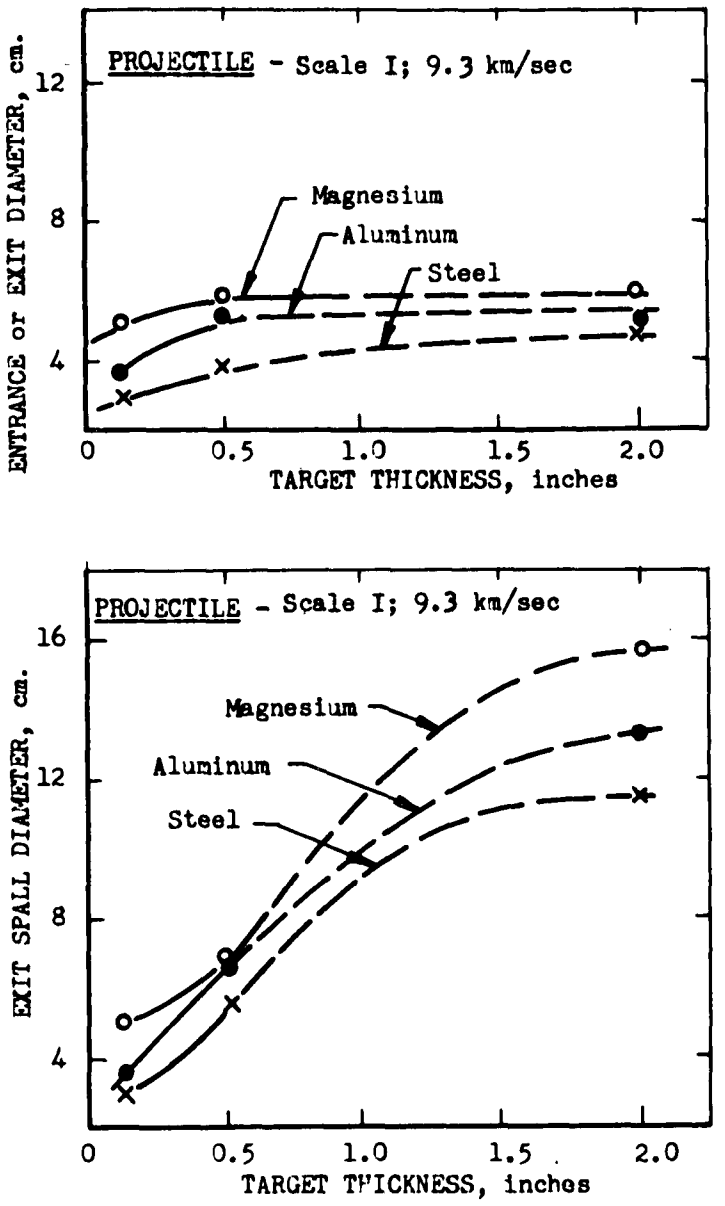

FIGURE 3. - Perforation and spall diameters vs. target thickness for several target materials impacted by 9.3 km/sec, inhibited jet projectiles.

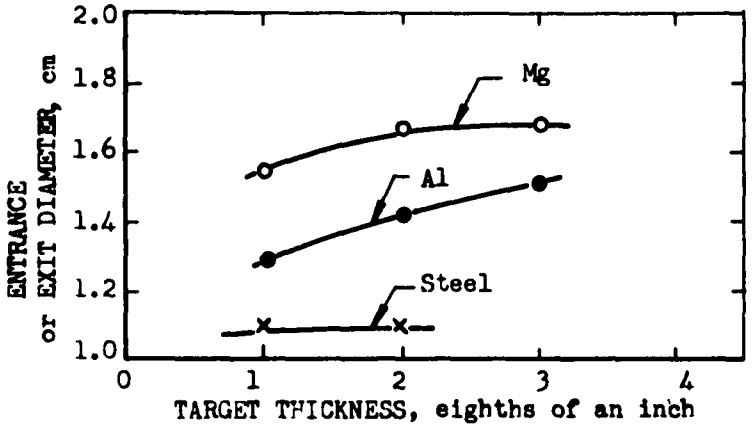

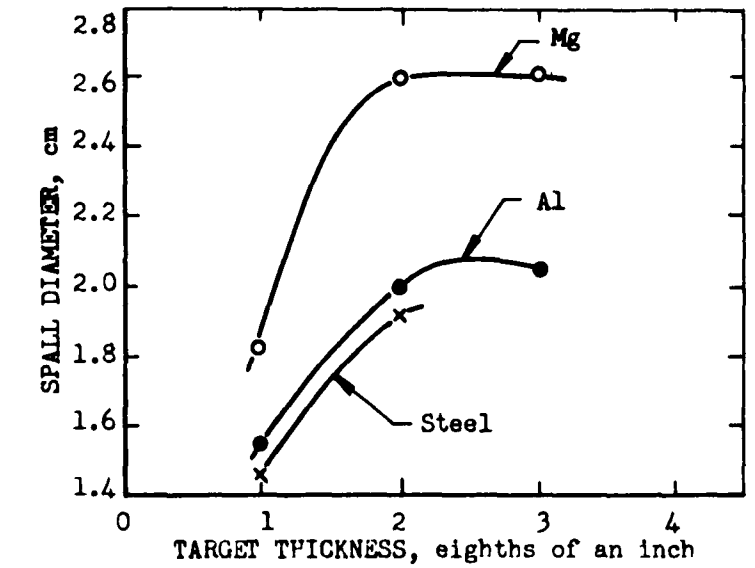

FIGURE 4. - Perforation and spall diameters vs. target thickness for several target materials impacted by 5.0 km/sec; 0.18 gm projectiles.

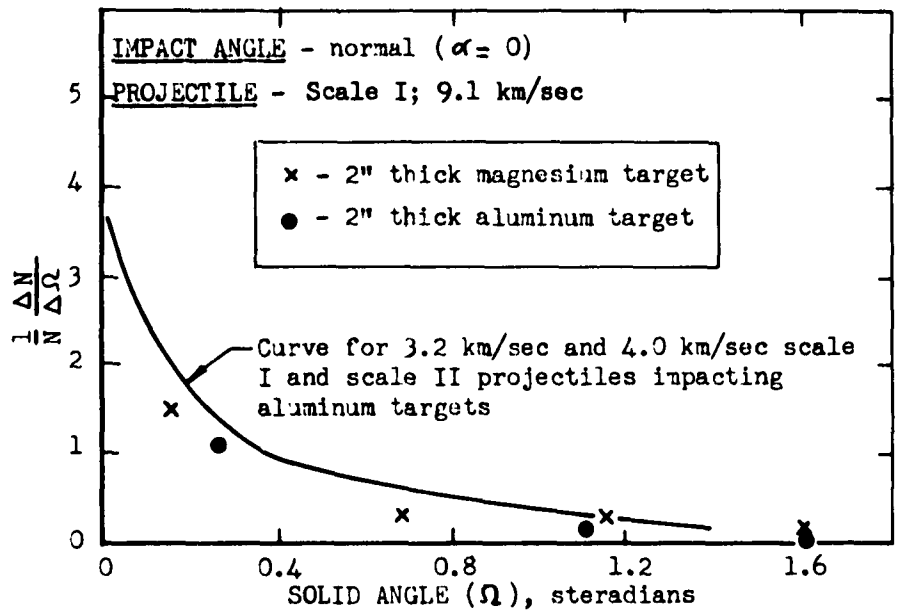

FIGURE 5. - Normalized distribution for target spall numbers.

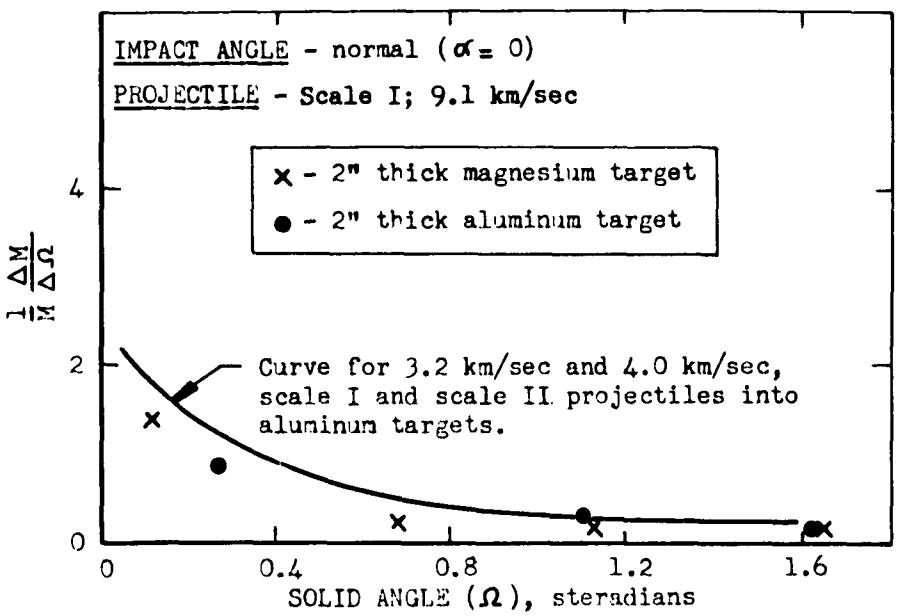

FIGURE 6. - Normalized distribution for target spall mass.

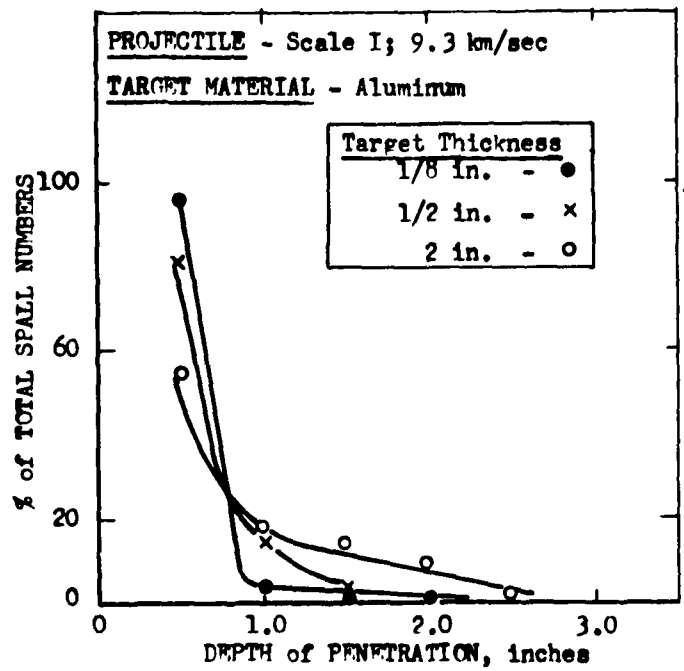

FIGURE 7. - Numbers of aluminum spall particles distributed according to depth of penetration into fiberboard.

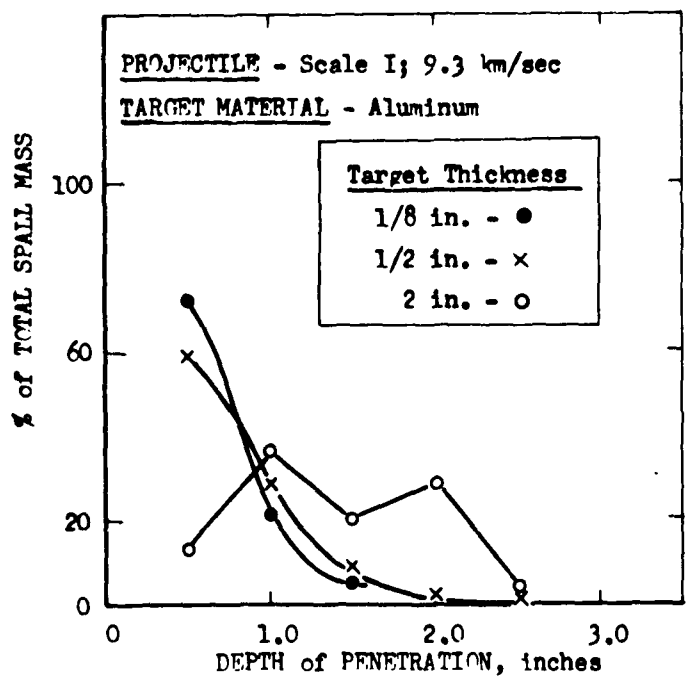

FIGURE 8. - Masses of aluminum spall particles distributed according to depth of penetration into fiberboard.

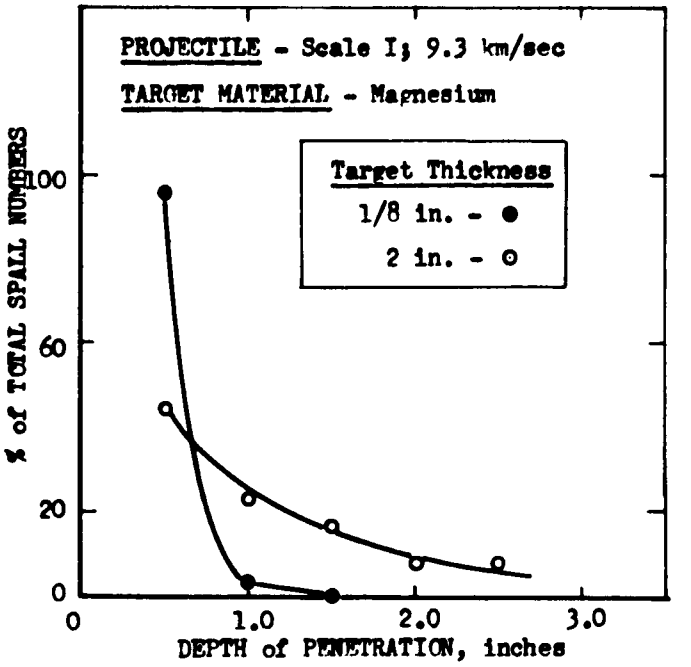

FIGURE 9. - Numbers of magnesium spall particles distributed according to depth of penetration into fiberboard.

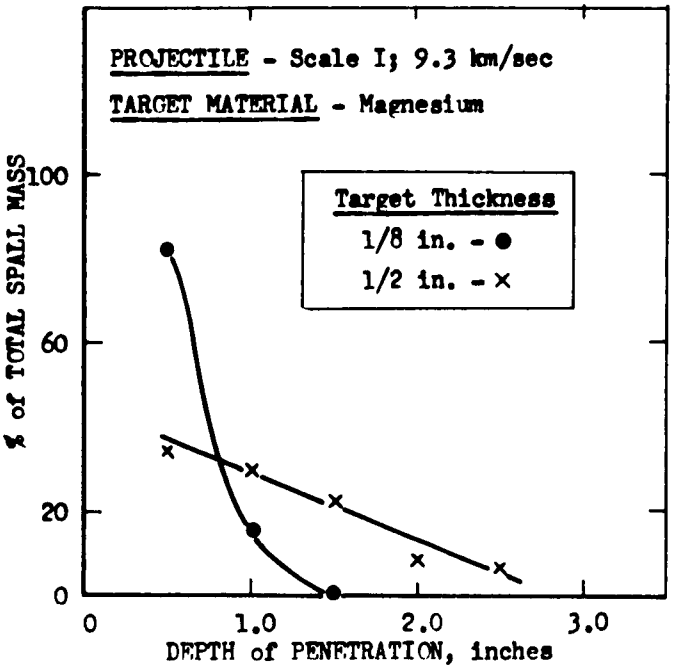

FIGURE 10. - Masses of magnesium spall particles distributed according to depth of penetration into fiberboard.

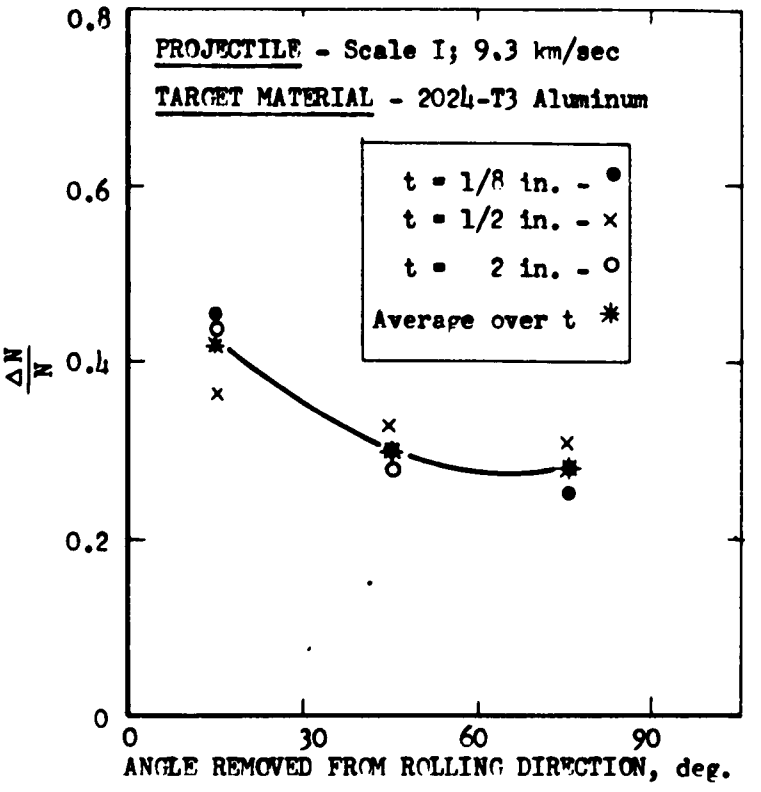

FIGURE 11. - Distribution of the number of spall particles as a function of angular distance removed from the direction the target plates were rolled in the fabrication process.

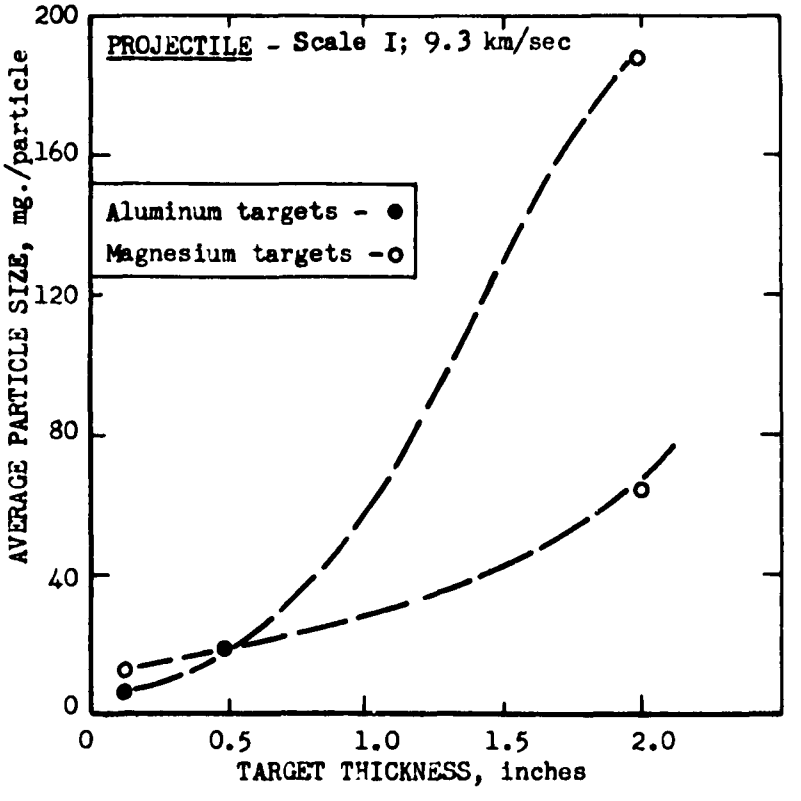

FIGURE 12. - Average spall particle size as a function of target thickness.

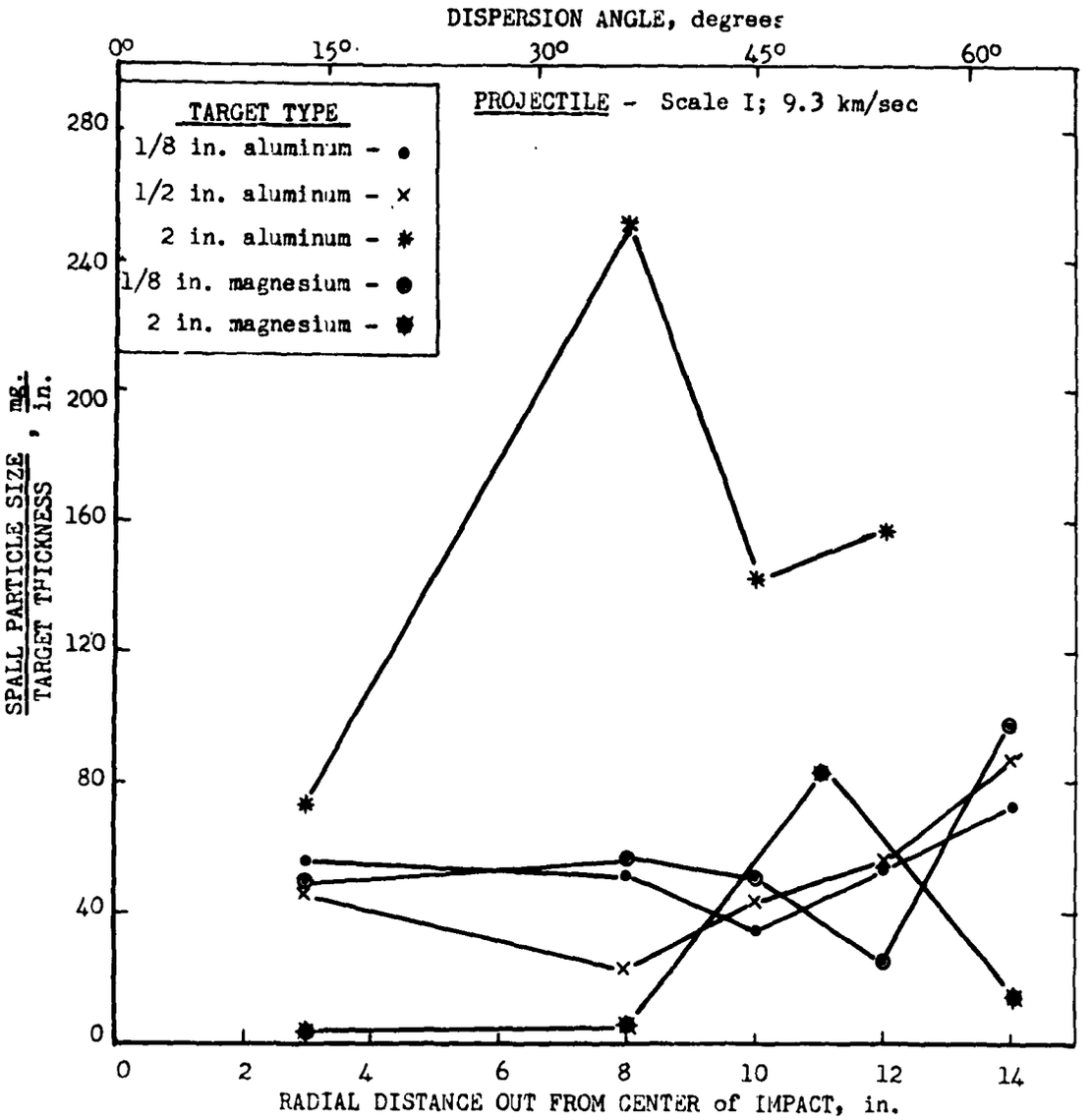

FIGURE 13. - Relationship between spall particle size and the outward direction in which spall particles were dispersed.

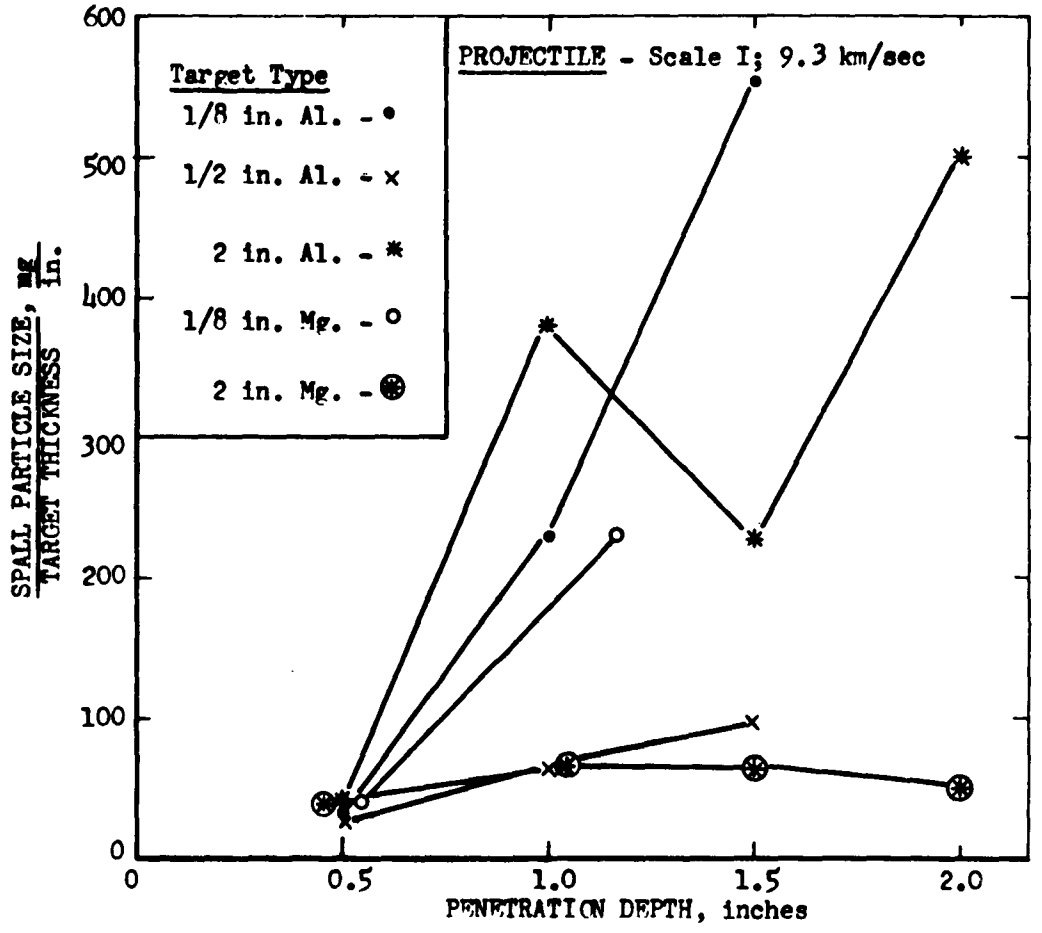

FIGURE 14. - Relationship between spall particle size and penetration depth into fiberboard recovery sheets.

DISTRIBUTION LIST FOR

Type I Quarterly Report

on

Hypervelocity Impact Phenomena

Sponsored by the Department of the Army
Aberdeen Proving Ground

Commanding General
Aberdeen Proving Ground
Maryland
Attn: F. E. Allison
Ballistic Research Laboratories

Commanding General
Aberdeen Proving Ground
Maryland
Attn: R. J. Eichelberger
Ballistic Research Laboratories

Commanding General
Aberdeen Proving Ground
Maryland
Attn: Technical Library
Ballistic Research Laboratories

Office, Chief of Ordnance
Department of the Army
Washington 25, D. C.
Attn: ORDTU

British Joint Services Mission
1800 K Street, N. W.
Washington 6, D. C.
Attn: Reports Officer

Commanding Officer
U. S. Naval Ordnance Test Station
China Lake, California
Attn: J. W. Rogers

Commanding Officer
Air Proving Ground Center
Eglin Air Force Base, Florida
Attn: H. L. Davis

Commanding General
Aberdeen Proving Ground
Maryland
Attn; S. Kronman
Ballistic Research
Laboratories

Commanding General
Aberdeen Proving Ground
Maryland
Attn: J. Kineke
Ballistic Research
Laboratories

Office, Chief of Ordnance
Department of the Army
Washington 25, D. C.
Attn: ORDTB, Ballistics Section
Mr. M. C. Miller

Commanding Officer
Armed Services Technical
Information Agency
Arlington Hall Station
Arlington 12, Virginia
Attn: TIPCR

Canadian Army Staff
2450 Massachusetts Avenue
Washington 8, D. C.

Director
U. S. Naval Research Laboratory
Washington 25, D. C.
Attn: Mr. W. W. Atkins, Code 130

Commanding Officer
Air Proving Ground Center
Eglin Air Force Base, Florida
Attn: Lt. W. H. Dittrich
Det. 4, ASD(ASQWR)

Director, The RAND Corporation
1700 Main Street
Santa Monica, California
Attn: J. H. Huth

Director, The RAND Corporation
1700 Main Street
Santa Monica, California
Attn: R. L. Bjork

Director, The RAND Corporation
1700 Main Street
Santa Monica, California
Attn: Technical Library

Library of Congress
Technical Information Division
Reference Department
Washington 25, D. C.
Attn: Bibliograph Section

General Motors Corporation
Defense Systems Div., Box T
Santa Barbara, California
Attn: J. W. Gehring

The Firestone Tire & Rubber Company
1200 Firestone Parkway
Akron, Ohio
Attn: C. M. Cox

Commanding Officer
Air Proving Ground Center
Eglin Air Force Base, Florida
Attn: F. E. Howard
Det. 4, ASD(ASQP)

Director, National Aeronautics &
Space Administration
Ames Research Center
Moffett Field, California
Attn: J. L. Summers

Director, National Aeronautics &
Space Administration
Ames Research Center
Moffett Field, California
Attn: Technical Library

Director, National Aeronautics &
Space Administration
Langley Research Center
Langley Field, Virginia
Attn: W. H. Kinard

Director, National Aeronautics &
Space Administration
Langley Research Center
Langley Field, Virginia
Attn: Technical Library

General Motors Corporation
Defense Systems Div., Box T
Santa Barbara, California
Attn: Technical Library

Aeroelastic & Structures
Laboratory
Massachusetts Institute of
Technology
77 Massachusetts Avenue
Cambridge 39, Massachusetts
Attn: W. Herrmann

Drexel Institute of Technology
Mechanical Engineering Dept.
Philadelphia 4, Pennsylvania
Attn: Pei Chi Chou

National Aeronautics and Space
Administration
Lewis Research Center
21000 Brookpark Road
Cleveland 35, Ohio

General Atomic Division
General Dynamics Corporation
P. O. Box 608
San Diego, California
Attn: J. M. Walsh

General Atomic Division
General Dynamics Corporation
P. O. Box 608
San Diego, California
Attn: M. F. Scharff

Flight Physics Laboratory
Defense Research Laboratory, Box T
General Motors Corporation
Santa Barbara, California
Attn: A. B. Wenzel

Pratt and Whitney Aircraft Division
United Aircraft Corporation
East Hartford, Connecticut
Attn: H. Kraus